IEEE Access
Multidisciplinary | Rapid Review | Open Access Journal

Received March 28, 2021, accepted April 14, 2021, date of publication April 22, 2021, date of current version April 29, 2021.

Digital Object Identifier 10.1109/ACCESS.2021.3075059

A Cooperative Autonomous Scheduling Approach for Multiple Earth Observation Satellites With Intensive Missions

JUNTONG QI[1], JINJIN GUO[1], MINGMING WANG[1], AND CHONG WU[2]
[1]School of Electrical and Information Engineering, Tianjin University, Tianjin 300072, China
[2]EFY Intelligent Control (Tianjin) Technology Company Ltd., Tianjin 300450, China

Corresponding author: Juntong Qi (qijt@tju.edu.cn)

This work was supported in part by the National Natural Science Foundation of China under Grant 61873182, and in part by the Science and Technology on Space Intelligent Control Laboratory under Grant HTKJ2019KL502009.

ABSTRACT Autonomous mission scheduling of multiple earth observation satellites (multi-EOSs) is considered as a complicated combinatorial optimization problem, which requires simultaneous consideration of imaging needs, resource constraints (electricity and memory) and possible emergencies. However, EOS resources are extremely scarce relative to intensive mission observation demands and most of the existing algorithms seldom consider emergencies. To address these challenges, this paper proposes a complete multi-EOSs scheduling scheme composed of two coupling stages, including mission pre-planning and mission replanning. We aim to obtain the optimal scheduling scheme for each EOS at the same time by maximizing the observation profits and balancing the resource consumption of each EOS. In this study, the roles of solar energy and ground stations in multi-EOSs mission scheduling are also considered. In the first stage, based on the cooperation and competition mechanism as well as the dynamic adjustment approach, an evolutionary ant colony optimization (EACO) method is developed to obtain the optimal solution for multi-EOSs pre-planning. In the second stage, using the results produced by EACO, we propose an interactive replanning approach to replan the missions that cannot be performed by faulty EOS in the event of unexpected accidents. Finally, several target scenarios are designed and numerical experiments are performed to show that the proposed algorithm presents better performance for large-scale multi-EOSs missions than other state-of-the-art algorithms.

INDEX TERMS Multiple earth observation satellites, autonomous mission scheduling, evolutionary ant colony optimization, dynamic adjustment approach, interactive replanning approach.

I. INTRODUCTION

Earth observation satellites (EOSs) can capture higher resolution images of the ground using optical sensors to obtain key information. EOSs can continuously observe areas of interest over a period of time, so they have been widely applied for ecology observation, disaster monitoring, national defense, and other fields [1]. With the increase in user demand and the occurrence of unexpected emergencies, EOSs need to be reasonably planned to respond to each mission quickly. However, the observation missions of EOSs have the characteristics of high cost and complex technological requirements. Reasonable planning and maximization of the observed profits are therefore key problems that need to be solved. At present, the cooperative operation of multiple EOSs (multi-EOSs) has been applied to several instances, including the German commercial satellite constellation RapidEye [2], the GPM mission deployed by NASA and JAXA [3], the QB50 mission launched by the European Union in 2011 [4] and Chinese BeiDou satellites [5].

The multi-EOSs scheduling problem involves many aspects, such as satellite resources, electricity consumption, data transmission, observation mission requests, and other factors that affect planning. Multi-EOSs scheduling is a multi-agent mission allocation problem and this research area has garnered increasing attention from scholars in recent years. Rizk *et al.* [6] discussed the challenges and future developments of multi-agent mission allocation and planning. Unlike general planning and scheduling problem, one of the main characteristics of multi-EOSs scheduling is

The associate editor coordinating the review of this manuscript and approving it for publication was Yichuan Jiang.

the visible time window (VTW) of each target, which is the time interval for which each target is visible to the EOSs. The EOSs can carry out observation missions only within the VTWs. A VTW is associated with the orbit parameters of the EOSs and the geographical location of targets. To address the problem of EOSs mission scheduling, some scholars adopted exact algorithms [7,8], although exact algorithms provide optimal solutions, they are only suitable for handling small-scale problems. There some scholars adopted heuristic algorithms and swarm intelligent optimization algorithms to deal with large-scale scheduling problems [9,10]. Darnopykh *et al.* [11] showed that EOSs scheduling is an NP-hard problem, and exact search algorithms are not suitable for the multi-EOSs scheduling problem. Tangpattanakul *et al.* [12] proposed an indicator-based multi-objective local search heuristic to solve the optimization problem associated with the selecting and scheduling of an EOS's observations. However, with the improvement of space technology, the number of deployed satellites is also increasing, and the scheduling of multiple satellites has become a popular topic of research for many scholars [13].

Multi-EOSs scheduling is an extension of single-EOS scheduling, and it is reasonable to handle multi-EOSs scheduling using heuristic algorithms. Refs. [14], [15] proposed a genetic algorithm (GA) to solve the satellite constellation optimal scheduling problem to minimize the system response time when performing large-area observation missions. Refs. [16], [17] used non-dominated sorting genetic algorithm-II (NSGA-II) to solve the multi-satellite mission planning problem for large-area image acquisition. Sarkheyli *et al.* [18] presented a new tabu search algorithm for resource scheduling of low earth orbit (LEO) satellites mission. To overcome the deficiencies in the static mission clustering, Wu *et al.* [19] presented an adaptive simulated annealing-based scheduling algorithm integrated with a dynamic mission clustering strategy for satellites observation scheduling. Zhang *et al.* [20], [21] proposed an ant colony optimization (ACO) to effectively plan various control resources for ensuring the normal operation of satellites. Yu *et al.* [22] proposed an improved cooperation-oriented ACO to solve the scheduling problem of aerial multi-target staring surveillance with multi-satellites. Besides, other algorithms, such as particle swarm optimization (PSO) [23], [24] and learning-based approach [25], [26], have been proposed to solve multi-satellite scheduling problems.

The above works have realized the importance of multi-satellite mission scheduling, and some researchers have further considered other factors, such as battery capacity [18], [27] and storage capacity [22], [28]. However, these works have ignored the roles of solar energy and ground station in mission scheduling. Although satellite resources are limited, they can be charged in regions receiving sunlight and can deallocate memory by transmitting observation data to the ground stations. Furthermore, the importance of data transmission is shown in the reference [29]. Owing to the complexity and large-scale of multi-EOSs scheduling, intelligent optimization algorithms are considered superior to exact algorithms in many aspects. Mosa *et al.* [30] showed that there are three aspects to choose ACO from intelligent algorithms to solve optimization problems. Firstly, ACO has a strong ability to solve optimization problems and could be easily understood. Secondly, the convergence of ACO has been proved. Thirdly, literature shows that ACO is superior to other intelligent search algorithms [31].

Furthermore, some emergencies, such as high-priority temporary observation missions or optical sensor failures, need to be considered in multi-EOSs mission scheduling. Therefore, optimal observation profits cannot be achieved if the observation missions are performed only according to the mission pre-allocated scheme. Motivated by the Refs. [32], [33], it is necessary to replan the scheduling of multi-EOSs online in the event of emergencies.

EOS resources are extremely scarce relative to intensive observation demands, so we need to design a reasonable cooperative observation scheme for multi-EOSs systems. However, to the best of our knowledge, very few studies are available on multi-EOSs scheduling where the imaging needs, resource constraints (electricity and memory) and possible emergencies are considered simultaneously. This paper mainly studies the observation of intensive missions and the mission replanning of faulty EOS. We propose a complete multi-EOSs scheduling scheme composed of two coupling stages: mission pre-planning and mission replanning. An improved ACO and an interactive replanning approach are proposed to solve the multi-EOSs autonomous mission scheduling. The main contributions of this work are as follows: (1) We introduce a dynamic two-stage strategy for multi-EOSs autonomous scheduling. The first stage is mission pre-planning, and the second stage is mission replanning. The second stage is based on the results of the first stage, which can greatly reduce the online computing time. The roles of solar energy and ground station in multi-EOSs mission scheduling are fully considered because satellite resources are recoverable via charging using solar energy and transmitting data to ground stations. (2) In the first stage, inspired by the rule of survival of the fittest, an evolutionary ant colony optimization (EACO) method based on cooperation and competition mechanism is proposed to solve the mission pre-planning of multi-EOSs. To further improve the convergence and increase the searchability of the algorithm, we propose a dynamic adjustment approach for information heuristic factor, expected heuristic factor and pheromone evaluation factor. (3) In the second stage, an interactive replanning framework is proposed for certain emergencies. In this framework, based on the interactive contract net protocol (ICNP), the mission load rate, exchange contract and dynamic mission insertion mechanism are introduced to address multi-EOSs mission replanning.

The remainder of this paper is organized as follows. Section 2 describes the multi-EOSs scheduling problem. In section3, the EACO is proposed which includes

cooperation and competition mechanism as well as the parameter dynamic adjustment approach. An interactive replanning framework is presented in Section 4. The simulation results are provided in Section 5. Finally, a conclusion is given in Section 6.

GPM	Global precipitation measurement
EOS	Earth observation satellites
Multi-EOSs	Multiple earth observation satellites
LEO	Low earth orbit
VTW	Visible time window
OTW	Observation time window
DW	Download window
STK	Satellite Tool Kit
UAV	Unmanned aerial vehicle
GA	Genetic algorithm
NSGA-II	Non-dominated sorting genetic algorithm-II
ACO	Ant colony optimization
PSO	Particle swarm optimization
EACO	Evolutionary ant colony optimization
ICNP	Interactive contract net protocol
TPGA	two-phase genetic annealing algorithm

II. PROBLEM DESCRIPTION

Due to the constraints of mobility and on-board resources, the observation capability of a single EOS is insufficient for intensive missions, so it is necessary to study the autonomous scheduling of multiple EOSs. Multi-EOSs scheduling mainly involves the planning of satellite resources, electricity consumption, data transmission, observation mission requests, among others. The actual target achieved by multi-EOSs mission scheduling is to allocate missions to each EOS reasonably and make full use of the resources of each EOS. Considering the constraints of actual observation, a group of executable missions is selected from the candidate missions for each EOS to maximize the total profits. Most studies on multi-EOSs scheduling have not considered the recoverability of EOSs resources. Besides, because of the emergency missions and EOS failure, it is necessary to reallocate the multi-EOSs missions online. Thus, this study considered multi-EOSs scheduling from these two aspects. A diagram of the multi-EOSs scheduling process is shown in Fig. 1.

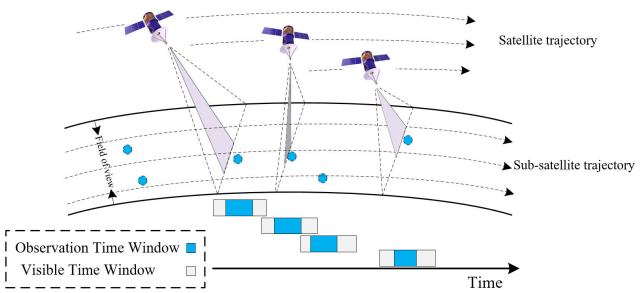

FIGURE 1. Schematic diagram of multi satellite observation mission.

A. VARIABLES

The main variables and parameters used in this work are defined as follows. Let $\boldsymbol{T} = \{T_i | i = 1, 2, \ldots, N_t\}$ be a set of missions, where T_i is a mission to be observed, N_t is the total number of missions. Here, the observation request of a ground target is regarded as a mission. For each mission T_i, some notations are defined to describe their characteristics.

- Tp_i: priority of the mission T_i
- Td_i: execution duration of the mission T_i
- Tm_i: memory occupation of the mission T_i
- Te_i: electricity consumption of the mission T_i
- θ_i: minimum elevation of the mission T_i

The set $\boldsymbol{G} = \{G_j | j = 1, 2, \ldots, N_g\}$ is defined as a set of ground stations, where N_g represents the total number of ground stations. The set of EOSs is defined as $\boldsymbol{S} = \{S_l | l = 1, 2, \ldots, N_s\}$, where Sal is an EOS, and N_s is the number of satellites. The resource of the l-th satellite can be defined as follows.

- $Small$, $Seals$: maximal memory and electricity capacity of EOS S_l, which reflects the ability of the EOS to observe the missions
- $infield$, $intimal$: initial electricity and memory of EOS S_l
- $rateDT_l$: data transmission rate between EOS S_l and each ground station
- $ecDT_l$: electricity consumption per unit of data transmission S_l
- $rateE_l$: charging rate of solar battery on EOS S_l

Multiple EOSs consume electricity when performing missions and communicating with the ground stations. In this paper, we consider that the solar batteries of EOSs would be charged in the sunshine areas of each orbit. The set $\boldsymbol{SR_l} = \{SR_1^l, SR_2^l, \ldots, SR_h^l\}$ is defined as the total sunshine area of EOS S_l, where $SR_h^l = \left[sunS_h^l, sunE_h^l\right]$ is the h-th sunshine area of EOS S_l, $sunS_h^l$ and $sunE_h^l$ are the start and end times of sunshine area SR_h^l. Let $\boldsymbol{TW_i^l} = \{TW_{i1}^l, TW_{i2}^l, \ldots, TW_{ik}^l\}$ be the set of all the VTWs for mission T_i by EOS S_l, where $TW_{ik}^l = \left[ts_{ik}^l, te_{ik}^l\right]$ is the k-th VTW of mission T_i by EOS Sal,ts_{ik}^l and te_{ik}^l are the start and end times for TW_{ik}^l. The duration of a VTW varies from tens of seconds to a few minutes. According to the user observation request, an appropriate time interval is selected from the VTW as the observation time window (OTW). The set $OW_{ik}^l = \left[os_{ik}^l, oe_{ik}^l\right]$ is the k-th OTW of mission T_i by EOS S_l, and some missions require multiple observations, so k>0. Similarly, we define the time interval when the EOSs are visible to a ground station as the download window (DW). The set $\boldsymbol{DW_j^l} = \{TW_{j1}^l, TW_{j2}^l, \ldots, TW_{js}^l\}$ as a DW of the j-th ground station G_j by EOS S_l, where $DW_{js}^l = \left[ds_{js}^l, de_{js}^l\right]$ is the s-th DW, ds_{js}^l and de_{js}^l are the start and end time for DW_{js}^l.

Furthermore, a binary decision variable is defined to decide whether the VTWs from the missions are chosen.

$$Tsel_{ik}^l \in \{0, 1\}, \forall S_l \in \boldsymbol{S}, T_l \in \boldsymbol{T}, TW_{ik}^l \in \boldsymbol{TW}_i^l \quad (1)$$

where $Tsel_{ik}^{l} = 1$ means that the TW_{ik}^{l} of mission T_i is selected by EOS S_l. If EOS S_l does not perform mission T_i, then $Tsel_{ik}^{l} = 0$. The mission of EOSs transmitting data to the ground stations is similar to the decision of performing the observation missions.

B. MATHEMATICAL MODELING

Although a target may need to be observed multiple times, each target can only be observed by one EOS in a given time period. The set $\boldsymbol{MS_i} = \{ms_{ik}^{l} | l = 1, 2, \ldots, N_s; k = 1, 2, \ldots\}$ indicates that the i-th mission is allocated to the l-th EOS, and the subscript k represents k-th OTW of the mission. The optimization goal of the multi-EOSs scheduling problem is to maximize the sum of the observation profits and ensure that the resource consumption of each EOS is relatively average, which can be expressed as follows:

$$Max \begin{cases} \boldsymbol{F_1} : (1-\omega_p) \sum_{l=1}^{Ns} F_p \\ \boldsymbol{F_2} : -\omega_p \sum_{l=1}^{Ns} (IdealRes_l - F_{c1} - F_{c2})^2 \end{cases} \tag{2}$$

$$\boldsymbol{s.t.} \begin{cases} \boldsymbol{a} : \forall ms_{ik}^{l}, ms_{ik}^{r} (l \neq r), ms_{ik}^{l} \cap ms_{ik}^{r} = \emptyset; \\ \boldsymbol{b} : 0 \leq infield - \sum_{i=1}^{Nt} \sum_{k=1}^{|TW_i^l|} Tsel_{ik}^{l} \cdot Te_i \\ + \sum_{h=1}^{|SR_l|} rateE_l \cdot SR_h^l - \sum_{j=1}^{Ng} \sum_{s=1}^{|DW_j^l|} ecDT_l \\ \cdot rateDT_l^l \cdot DW_{js}^{l} \leq Seals; \\ \boldsymbol{c} : 0 \leq iniD_l - \sum_{i=1}^{Nt} \sum_{k=1}^{|TW_i^l|} Tsel_{ik}^{l} \cdot Tm_i \\ + \sum_{j=1}^{Ng} \sum_{s=1}^{|DW_j^l|} rateDT_l^l \cdot \left(DW_{js}^{l}\right) \leq SD_l; \\ \boldsymbol{d} : \begin{cases} oe_i k^l + trans(i, i+1) \leq os_{i+k,k}^{l} \\ trans(i, i+1) = \varphi_i^l - \varphi_{i+1}^l / v_{\varphi_i}^l + stime^l \end{cases} \\ \boldsymbol{e} : \begin{cases} ts_{ik}^{l} \leq os_{ik}^{l} \leq oe_{ik}^{l} \leq te_{ik}^{l}, oe_{ik}^{l} - os_{ik}^{l} \geq Td_i \\ os_{ik}^{l} \leq ts_{ik}^{l} \leq te_{ik}^{l} \leq oe_{ik}^{l}, te_{ik}^{l} - ts_{ik}^{l} \geq Td_i \\ ts_{ik}^{l} \leq os_{ik}^{l} \leq te_{ik}^{l} \leq oe_{ik}^{l}, te_{ik}^{l} - os_{ik}^{l} \geq Td_i \\ os_{ik}^{l} \leq ts_{ik}^{l} \leq oe_{ik}^{l} \leq te_{ik}^{l}, oe_{ik}^{l} - ts_{ik}^{l} \geq Td_i \end{cases} \end{cases} \tag{3}$$

where i is the index of mission $\boldsymbol{T}$, k is the index of VTWs, l is the index of EOSs $\boldsymbol{S}$, ω_p is the weight coefficientweight coefficientweight coefficient, $IdealRes_l$ is the ideal consumption resource of the l-th EOS, which depends on the total available resources of that EOS, $F_p = \sum_{i=1}^{Nt} \sum_{k=1}^{|TW_i^l|} Tsel_{ik}^{l} \cdot Tp_i$ is the total priority of observation targets, $F_{c1} = \sum_{i=1}^{Nt} \sum_{k=1}^{|TW_i^l|} Tsel_{ik}^{l} (Tm_i + Te_i)$ include the electricity and memory consumed for multi-EOSs observation, $F_{c2} = \sum_{i=1}^{Nt} \sum_{j=1}^{Ng} \sum_{s=1}^{|DW_l^l|} ecDT_l \left(DW_j^l\right)$ is the electricity consumption of the multiple EOSs transmitting data to ground station, $\sum_{j=1}^{Ng} \sum_{s=1}^{|DW_l^l|} ecDT_l \left(DW_j^l\right)$ is the amount of data released for transmission to the ground stations, $\sum_{h=1}^{|SR_l|} rateE_l \cdot \left(SR_h^l\right)$ is the total amount of charging in the sunshine region, φ_i^l is the look angle of mission T_i, v_{φ}^{l} is sensor's slewing velocity and $stime^l$ is the recover time of sensor slewing.

Objective Function (2) consists of two parts $\boldsymbol{F_1}$ and $\boldsymbol{F_2}$: $\boldsymbol{F_1}$ is to maximize the sum of the priorities of observation missions; $\boldsymbol{F_2}$ ensures that the resources consumed by each EOS are relatively average. Thus, an EOS with abundant resources can perform more missions, while that with few resources can perform fewer missions. Here, priority is given to maximizing $\boldsymbol{F_1}$ to ensure that more and more important missions are observed.

Equation (3) is the constraint to be considered in the observation scheduling. Equation (3a) is the mission execution constraint indicating that a given mission can only be allocated to one EOS in a given time period to avoid wastage of resources caused by mission conflicts. The i-th mission can only be allocated to one EOS in a given time interval k.

Equation (3b) is the electricity constraint, which represents the electricity consumed by the EOSs for image acquisition and data transmission and that the electricity supplied by solar batteries needs to meet the limits of the battery capacity.

Equation (3c) is the memory constraint, which indicates that the EOS memory should always be within its safe range during data collection and transmission.

Equations (3d) is the maneuver constraint, which indicates that the EOS must have enough time to adjust and stabilize the swing angle of the sensor when performing the continuous observation missions.

Equations (3e) is the time constraint, which indicates that the observation duration needs to meet user requirements and that the mission can only be observed in the VTWs.

The flowchart of the multi-EOSs scheduling proposed is illustrated in Fig. 2.

III. OPTIMAL MISSION PRE-PLANNING SCHEME BASED ON EACO ALGORITHM

To reduce the time consumed during multi-ESOs scheduling and achieve optimal allocation, we established the cooperative competition rules between the ant colony based on survival of the fittest. Then, to prevent the algorithm from converging to a local optimal solution too quickly, the state transition and pheromone update rules are designed based on the elite ant system. Thereafter, a parameter dynamic adjustment approach is constructed in combination with the multi-EOSs scheduling problem. The mission pre-planning algorithm is shown in Algorithm 1.

A. STATE TRANSITION RULE

According to the selection probability of the candidate missions, the state transition rule selects the optimal mission

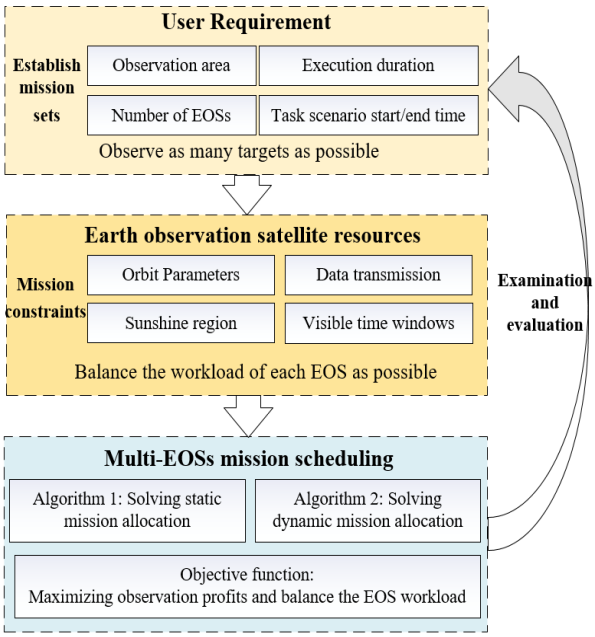

FIGURE 2. Framework of multi-EOSs mission scheduling.

sequence for each EOSs using a certain method, to maximize the observation profits. The following is an example of selecting the next mission T_k from a set of missions after performing mission T_i. The pheromone on EOS S_l performing mission T_i and mission T_k is define as $\tau_{ik,t}$. Then, the probability of selecting mission T_k is given as follows:

$$k = \begin{cases} arg \ \max\limits_{s \in \bar{m}_l} \{ \left[\tau_{is,t}^{\alpha_t} \right] \left[\eta_{s,t}^{\beta_t} \right] \}, & C_{T,t} \le q_0 \\ p_{ik,t}^{l}, & otherwise \end{cases} \tag{4}$$

where t is the iteration number, α_t is the information heuristic factor that represents the importance of the pheromone, β_t is the expected heuristic factor that indicates the importance of heuristic information. $\bar{m}_l$ represents the set of remaining candidate missions of the EOS S_l, η_s represents the heuristic information of mission T_s, q_0 is a parameter between 0 and 1, and $C_{T,t}$ is a number of uniform distribution that controls the transfer rules.

In the traditional ACO, the random selection threshold $C_{T,t}$ is a random number on [0,1], which causes chaos of the solution. In this work, the random selection threshold $C_{T,t}$ is controlled by the uniform random number on [0,1]. The uniform distribution is chosen here to ensure that the choice of search optimization strategy for each iteration is equally possible and to increase the randomness of the solution more reasonably. According to the expression of uniform distribution function, we can get the expression of $C_{T,t}$ as follows:

$$C_{T,t} = \begin{cases} C_{T,t} / \kappa_c, & C_{T,t} \in (0, \kappa_c) \\ \left(C_{T,t} - \kappa_c \right) / \left(1 - \kappa_c \right), & C_{T,t} \in (\kappa_c, 1) \end{cases} \tag{5}$$

where $\kappa_c \in (0, 1)$ determines the change frequency of $C_{T,t}$ and the state transition probability $p_{ik,t}^{l}$ is designed as follows:

$$p_{ik,t}^{l} = \begin{cases} \dfrac{\left[\tau_{ik,t}^{\alpha_t} \right] \left[\eta_{k,t}^{\beta_t} \right]}{\sum_{s \in \bar{m}_l} \left[\tau_{is,t}^{\alpha_t} \right] \left[\eta_{s,t}^{\beta_t} \right]}, & k \in \bar{m}_l \\ 0, & otherwise \end{cases} \tag{6}$$

B. PHEROMONE UPDATE RULE

The pheromone update process includes evaporation and generation of pheromones. To avoid search stagnation, this work first introduces the elite ant colony system that releases additional pheromones to enhance the effects of positive feedback. Second, the pheromone concentration of each mission sequence has a maximum and a minimum. Because the minimum concentration is conducive for better solution exploration, the maximum concentration ensures that the experience is enlightening for the ant colony. The local pheromone update rule is as follows:

$$\begin{cases} \tau_{ik,t} = (1 - \rho_t) \, \tau_{ik,t} + \Delta \tau_{ik,t} \\ \Delta \tau_{ik,t} = \sum_{a=1}^{n} Ant \dfrac{Q_\tau}{Fun_a} \\ nAnt = \kappa_n \cdot num(SeleT) \end{cases} \tag{7}$$

where ρ_t is the pheromone evaporation factor that is used to prevent infinite accumulation of pheromones, and its value range is 0 to 1; $\Delta \tau_{ik,t}$ is the accumulation of the pheromone concentration on the mission sequence from mission T_i to mission T_k for each ant at the end of the iteration t; $nAnt$ is the number of ants, which is determined by the number of candidate missions to be performed for each EOS; $SeleT$ is the set of candidate missions; Q_τ is pheromone amount and Fun_a is the objective function value obtained by ant a. After all the ants find the end node, the global pheromone update rule is performed by adding pheromones to all the edges, including the pheromones produced by the elite ants. The global update rule is described as follows:

$$\begin{cases} \tau_{ik,t+1} = (1 - \rho_t) \, \tau_{ik,t} + \rho_t \Delta \tau_{ik,t}^{*} \\ \Delta \tau_{ik,t}^{*} = \dfrac{Q_\tau}{Fun_{best}} \end{cases} \tag{8}$$

where $\Delta \tau_{ik,t}^{*}$ is the pheromone produced by elite ants. Then updated pheromone $\tau_{ik,t+1}$ is within range $[\tau_{min}, \tau_{max}]$.

C. DESIGN OF HEURISTIC FUNCTION FOR MULTI-EOSs SCHEDULING

Different objective functions represent different expectations for multi-EOSs scheduling, so the heuristic functions should also be designed according to the objective functions. The heuristic functions selected herein include mission priority, electricity consumption, and memory consumption.

In multi-EOSs scheduling, missions with higher priorities are considered first, and the mission resource consumption also reflects the scheduling rules of mission priority. Priority is given to missions that consume the fewest resources

because EOSs can conserve resources to accomplish more missions.

$$\begin{cases} p\eta_i = (Tp_{max} - Tp_i)\,(Tp_{max} - Tp_{min})^{-1} + \eta_1 \\ e\eta_i = (Te_{max} - Te_i)\,(Te_{max} - Te_{min})^{-1} + \eta_2 \\ m\eta_i = (Tm_{max} - Tm_i)\,(Tm_{max} - Tm_{min})^{-1} + \eta_3 \end{cases} \tag{9}$$

where Tp_{max} and Tp_{min} are the maximum and minimum of mission priority Tp_i; Te_{max} and Te_{min} are the maximum and minimum of electricity consumption in the mission set; Tm_{max} and Tm_{min} are the maximum and minimum of memory consumption in the mission set; η_1, η_2 and η_3 are small constants.

Based on the above heuristic information, the heuristic function for the EACO is obtained as follows:

$$\eta_i = \omega_1 \cdot p\eta_i + \omega_2 \cdot e\eta_i + (1 - \omega_1 - \omega_2) \cdot m\eta_i \tag{10}$$

where ω_1 and ω_2 are weight coefficients, indicating the importance of the mission properties.

D. COOPERATION AND COMPETITION STRATEGY

In nature, some animals cooperate to resist natural enemies, but they also compete with each other for food and territory. The cooperation and competition mechanisms make populations evolve toward better directions. The implementation principle for the evolutionary ACO based on cooperation and competition involves establishing an environment of cooperation and competition among the populations to find the optimal solution. The cooperation and competition mechanisms can be described as follows.

First, we define a cooperation coefficient; if the condition of information exchange among the ant colonies is satisfied, each ant colony will not exchange information randomly. Instead, information exchange is determined by the cooperation coefficient, which reflects its evolution characteristics. This not only avoids randomness but also ensures that pheromones will not gather on some paths, which effectively prevents the algorithm from converging prematurely. The cooperation coefficient of the r-th ant colony Co_r is defined as follows:

$$Co_r = \frac{Fun^r_{best}}{Fun^r_{avg}} \tag{11}$$

where Fun^r_{best} is the best objective function value in the r-th population, Fun^r_{avg} is the average value of the objective function in the r-th population. After g iterations, two ant subgroups are selected to exchange information according to cooperation probability, which is described as follows:

$$P_{co} = |Co_r - Co_k|, k = r-1, \ldots, r-g+1 \tag{12}$$

After the information exchange object of the r-th ant subgroup is determined as that of the k-th ant subgroup, the best solution of the k-th ant subgroup is replaced by the worst solution of the r-th ant subgroup.

$$Seq^r_{worsr} = Seq^k_{best} \tag{13}$$

where Seq^r_{worsr} is the worst mission scheduling result of r-th ant subgroup and Seq^k_{best} is the best mission scheduling result of k-th ant subgroup.

Algorithm 1 Mission Pre-Planning Based on EACO

Input: The set of EOSs $\boldsymbol{S}$, the set of missions $\boldsymbol{T}$, the set of ground station $\boldsymbol{G}$;
Output: Scheduling results of each EOS $\boldsymbol{PT}$;

Initialization: Schedule time horizon S_{day}, heuristic factor α_0, α_{min}, β_0, β_{min}, pheromone evaporation factor ρ_0, ρ_{min}, pheromone range τ_{min}, τ_{max}, parameters of selection threshold κ_c, $C_{T,0}$ and pheromone amount Q_τ, maximum iteration M_g;
for $l = 1; l \le N_s; l++$ **do**
  VTWs $\leftarrow$ **FunTW** ($\boldsymbol{S}$,$\boldsymbol{T}$,S_{day}) {*obtain VTWs*};
  $Count = 0$;
  while $TimeUnit(Count) \le S_{day}$ **do**
    for $i = 1; i \le N_t; i++$ **do**
      $SeleT \leftarrow$ **FunTask**(VTWs,T_i,Sal) {*Eq.* (3)};
    end for
    for $i = 1; i \le N_t; i++$ **do**
      if *Eq.* (19) *is satisfied* **then**
        $\alpha_t \leftarrow$ **Funalp**(α_{t-1}, κ_α,α_{min}) {*Eq.* (15)};
        $\beta_t \leftarrow$ **Funbeta**(β_{t-1}, κ_β,β_{min}) {*Eq.* (16)};
      end if
      if *update condition of* ρ_t *is satisfied* **then**
        $\rho_t \leftarrow$ **Funrho**(ρ_{t-1}, κ_ρ,ρ_{min}) {*Eq.* (17)};
      end if
      $k \leftarrow$ **Funtra**($\tau_{ik,t}$,$C_{T,t}$,α_t,β_t) {*Eq.* (4) $-$ (6)};
      $\tau_{ik,t+1} \leftarrow$ **Funtau**($\tau_{ik,t}$,ρ_t,κ_n,Q_τ,$SeleT$) {*Eq.* (7) $-$ (8)};
      $Seq_l \leftarrow$ allocate T_i to S_l {*Eq.* (11) $-$ (13)};
      $Res_l \leftarrow$ **Funres**(Sal,Seq_l,T_i);
    end for
    $Count = Count + 1$;
  end while
  $\boldsymbol{PT} \leftarrow$ **Funpt**($\boldsymbol{S}$,$\boldsymbol{T}$,Seq,Res);
end for

E. PARAMETER DYNAMIC ADJUSTMENT APPROACH

The ACO performance is not only related to the pheromone update rule and heuristic function but also affected by heuristic factors, pheromone evaporation factors, and other parameters. In the general ACO, the above parameters are fixed in the search process, which causes the algorithm to converge to the local optimum. Thus, we propose a parameter dynamic adjustment approach based on the multi-EOSs scheduling problem. In the early stage, the approach mainly adjusts the heuristic factor, and in the later stage, it mainly adjusts the pheromones. To reduce unnecessary updates of the heuristic factor, a trigger condition for updating parameters is designed. That is, after g iterations, the heuristic factors are adjusted when the condition is satisfied. This update condition is defined as follows.

$$\mathbb{F}_t - \mathbb{F}_t - 1 \le \delta_h \mathbf{1}_g \tag{14}$$

where $\mathbb{F}_t = [Fun_{best,t-g+1}, \ldots, Fun_{best,t}]$, δ_h is the error threshold, and $\mathbf{1}_g$ is a p-dimensional column vector whose elements are all 1. When the above condition is satisfied, the updating rules of heuristic factors are as follows:

$$\alpha_t = \begin{cases} \kappa_\alpha \alpha_{t-1}, \ if \ \kappa_\alpha \alpha_{t-1} > \alpha_{min} \\ \alpha_{min}, \ otherwise \end{cases} \tag{15}$$

$$\beta_t = \begin{cases} \kappa_\beta \beta_{t-1}, \ if \ \kappa_\beta \beta_{t-1} > \beta_{min} \\ \beta_{min}, \ otherwise \end{cases} \tag{16}$$

where κ_α and κ_β are positive constants, and their main function is to change the heuristic factors from the optimal parameters of the earlier iteration to those of the later iteration; α_{min} and β_{min} are the minimum value of information heuristic factor and expectation heuristic factor.

If the objective function remains unchanged for g successive iterations, the algorithm may fall into a local optimal solution. Therefore, the pheromone evaporation factor is updated as follows:

$$\rho_t = \begin{cases} \kappa_\rho \rho_{t-1}, & if \ \kappa_\rho \rho_{t-1} > \rho_{min} \\ \rho_{min}, & otherwise \end{cases} \tag{17}$$

where κ_ρ is a positive constant, ρ_{min} is the minimum of pheromone evaporation factor.

Algorithm 2 Mission Replanning Based on Interactive Replanning Approach

Input: The set of EOSs $\boldsymbol{S}$, the set of missions $\boldsymbol{T}$, the set of ground station $\boldsymbol{G}$,the plan of mission allocation $\boldsymbol{PT}$, the failed EOSs F_s;

Output: Replanning results of each EOS $\boldsymbol{rePT}$;

Initialization: Schedule time horizon S_{day}, heuristic factor α_0, α_{min}, β_0, β_{min}, pheromone evaporation factor ρ_0, ρ_{min}, pheromone range τ_{min}, τ_{max}, parameters of selection threshold κ_c, $C_{T,0}$ and pheromone amount Q_τ, maximum iteration M_g;
$num_{Fs} \leftarrow num(F_s)$ {*the number of* F_s};
for $i = 1; i \leq num_{Fs}; i++$ **do**
  $task_{Fs} \leftarrow$ **Funtask** (F_s,$\boldsymbol{PT}$) {*tasks set of* F_s};
  $num_{taskFs} \leftarrow num\ (task_{Fs})$;
  for $j = 1; l \leq num_{taskFs}; j++$ **do**
    $WorkL \leftarrow$ **Funwk**($\boldsymbol{PT}$,$\boldsymbol{T}$,$AvaRes$) {*Eq.* (18)};
    $LoadIndex \leftarrow sort\ (WorkL,W)$ {*Eq.* (19)};
    for $l = 1; l \leq N_s; l++$ **do**
      if $LoadIndex\ (l) \neq F_s\ (i)$ **then**
        $reSeq_l \leftarrow$ allocate mission $task_{Fs}(j)$ to EOS $LoadIndex(l)$;
        $Pro_l \leftarrow$ **Funpr**($reSeq_l$, $\boldsymbol{S}$) {*obtain profit*};
      end if
    end for
    $\boldsymbol{rePT} \leftarrow$ **FunrPT**(Pro,$reSeq$,$\boldsymbol{S}$, $\boldsymbol{T}$) {*allocate to the highest profits EOS*};
  end for
end for

IV. MULTI-EOSs INTERACTIVE REPLANNING FRAMEWORK

When multiple EOSs perform observation missions, they may encounter unforeseen situations, such as optical equipment failure and temporary emergencies. Therefore, an interactive replanning approach for emergencies is also presented. Based on the results of mission pre-planning, the ICNP and mission insertion mechanisms are adopted to solve the mission replanning problem for multiple EOSs. The mission replanning algorithm is shown in Algorithm 2.

A. INTERACTIVE CONTRACT NET PROTOCOL

In the process of multi-EOSs scheduling, mission pre-planning requires a lot of time. If the condition for mission replanning is triggered, it is inappropriate to overturn the previous allocation scheme. Therefore, it is more appropriate to reallocate new missions on the basis of mission pre-planning. The interactive replanning approach has good adaptability and robustness for large-scale distributed systems. Multiple EOSs perform new missions according to the information exchange between each node until the system returns to a stable state. Then, they continue to perform missions or the next replanning. The negotiation process of the ICNP can be divided into the following four stages, namely bidding, participating in the bidding, winning the bid, and executing the contract, as shown in Fig. 3.

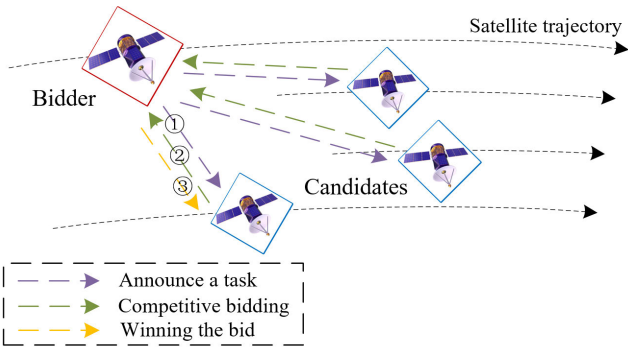

FIGURE 3. Schematic diagram of Interactive contract net protocol.

For new missions, an EOS with a lower workload is prioritized in the bidding stage. If this EOS cannot complete the mission, it will communicate with a potential candidate in the form of broadcasts as the bidder, informing them of the geographic location, time window, observation duration, and resources required to complete the new mission. In the event of EOS optical sensor failure, the EOS broadcasts mission information that cannot be completed (communication link will not fail), and the candidate EOSs then participate in the bidding for the new mission. Here, we define the workload of the l-th EOS as follows:

$$WorkL_l = \frac{\left[AvaRes_l - \sum_{i=1}^{Nt} \sum_{k=1}^{|TW_i^l|} Tsel_{ik}^l \ (Te_i + Tm_i) \right]}{AvaRes_l} \tag{18}$$

where is $AvaRes_l$ the available resource of the l-th EOS. If the EOS workload is greater than W_l, it means that the EOS is not suitable for new missions. For an EOS with a low workload, it judges whether the new mission can be inserted into the original mission list. The winning EOS is then determined by evaluating the profits of the candidate EOS performing the new missions.

$$\begin{cases} WorkL_l > W_l, & Not\ suitable\ for\ new\ tasks \\ WorkL_l \leq W_l, & It\ is\ possible\ to\ perform\ new\ tasks \end{cases} \tag{19}$$

where W_l is the threshold to judge whether the workload of the healthy EOS can perform new missions.

B. EXCHANGE CONTRACT AND MISSION INSERTION MECHANISM

The traditional replanning strategy arranges new missions at the end of the mission list, so it cannot guarantee maximum benefit from the missions. The exchange contract and mission insertion mechanism proposed herein is shown in Fig. 4 and implies that the reallocated mission is added to the vacant time of the healthy EOS. If the new mission has a higher priority, it will replace the original mission and maximize the benefit of the entire multi-EOSs system.

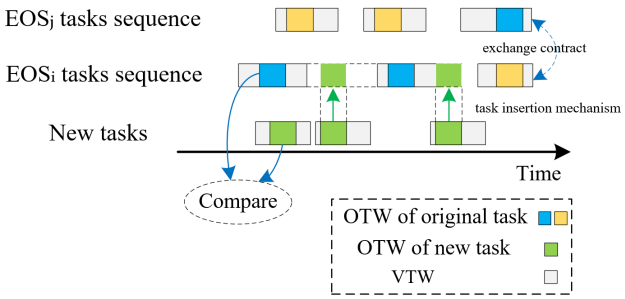

FIGURE 4. Schematic diagram of mission insertion mechanism.

V. RESULTS

In this section, we present some numerical and unmanned aerial vehicle (UAV) flight experiments to prove the effectiveness of the proposed algorithm. All the simulation data from the satellites and targets were obtained from Satellite Tool Kit (STK) 11.2. STK can be used to obtain the VTWs between the EOSs and the ground targets, the sunshine region of EOSs, and the DWs between the EOSs and ground stations. The schedule time horizon is 24 h, from 2020/12/25 00:00:00 to 2020/12/26 00:00:00. The design of the EOSs is shown in Fig. 5, and their orbit parameters are obtained from `https://celestrak.com/`. The experiment is coded in MATLAB R2018b and executed on a laptop with Intel(R) Core(TM) i5-8250U CPU (1.6 GHz) under Windows 10 with 16 GB RAM. The specific parameters are listed in Appendix A.

To verify the effectiveness of the algorithm, eight scenarios are designed here, and the number of ground targets is 25, 50, 75, 100, 125, 150, 175 and 200 respectively. The priority of

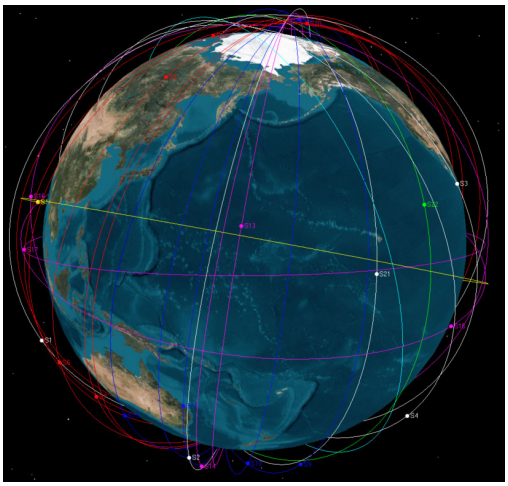

FIGURE 5. Orbits distribution of the 24 EOSs and specific parameters are listed in Appendix A.

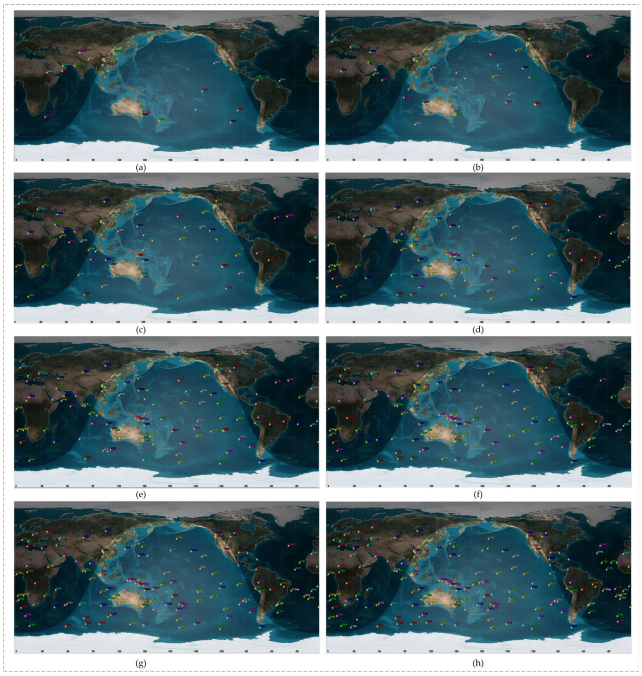

FIGURE 6. Illustration of target distribution scenarios. (a) Centralized: 2 target groups, each group has 5 targets; Random: 15 targets; (b) Centralized: 3 target groups, each group has 7 targets; Random: 29 targets; (c) Centralized: 4 target groups, each group has 8 targets; Random: 43 targets; (d) Centralized: 4 target groups, each group has 10 targets; Random: 60 targets; (e) Centralized: 5 target groups, each group has 10 targets; Random: 70 targets; (f) Centralized: 5 target groups, each group has 12 targets; Random: 90 targets; (g) Centralized: 5 target groups, each group has 15 targets; Random: 100 targets; (h) Centralized: 5 target groups, each group has 15 targets; Random: 125 targets.

ground targets is a random integer between 1 and 10. There are two types of ground targets and their location distribution is shown in Fig. 6. Two different types of targets are designed as follows:

1) The first one is centralized. In the eight scenarios, 2, 3, 4, 4, 5, 5, 5 and 5 cities are selected around the world. 5,

TABLE 1. Cities information.

ID	Name	Longitude(deg)	Latitude(deg)
1	Chengdu	104.06	30.67
2	Sydney	150.88	-33.92
3	Vancouver	-123.0	49.22
4	State of Malacca	100.02	3.57
5	New York	-74.03	40.78

TABLE 2. Ground station information.

Name	Longitude(deg)	Latitude(deg)	Elevation(deg)
Miyun	116	40	15
Kashi	75.93	39.51	15
Kunming	102.73	25.05	15
Sanya	109.50	18.20	15

7, 8, 10, 10, 12, 15 and 15 targets are generated within a 4° latitude and longitude of each city. The information of the five cities is shown in Table 1.

2) The second one is a global randomness. In the eight scenarios, 15, 29, 43, 60, 70, 90, 100 and 125 targets are generated, and their latitudes vary from - 60° to 60°.

The priority of each target is between 1 and 10, and the elevation angle is evenly distributed between 30° and 50°. The memory consumption and observation time of each target are evenly distributed between [300 MB, 350 MB] and [100 s, 120 s], respectively. The power consumption of each mission is positively correlated with the required observation time. The ground station information is shown in Table 2. The initial electricity and initial memory of each EOS are one-fourth of their total values.

A. PARAMETER ANALYSIS

The parameters of the EACO are shown in Table 3. To analyze the influence of different parameter combinations of heuristic factors on the early iteration results, we choose from $\alpha \in [1, 2]$ and $\beta \in [1, 2]$ with an interval of 0.05 respectively, and repeat the calculation 20 times for each parameter combination. The number of iterations is 10, and the result is as follows.

TABLE 3. Parameters of EACO.

Variable	Description	Value
M_g	Maximum iteration	80
α_{min}	Lower bound of information heuristic factor	1
β_{min}	Lower bound of expected heuristic factor	1
ρ_{min}	Lower bound of pheromone evaporation factor	0.01
Q_τ	Pheromone amount	600
τ_{min}	Lower bound of pheromone	0.05
τ_{max}	Upper bound of pheromone	0.95
κ_c	Control parameter of selection threshold	0.75
κ_n	Parameter for determining the number of ants	3

To analyze the influence of different heuristic factors on the later stage of the algorithm, the number of iterations is 80. The results are shown in Fig. 8.

From the simulation results of Fig. 7 and Fig. 8, we can get the appropriate heuristic factor parameter combination for the early and late iterations of multi-EOSs mission scheduling. The blue parts indicate that the average values of the objective functions were small, implying that the algorithm did not

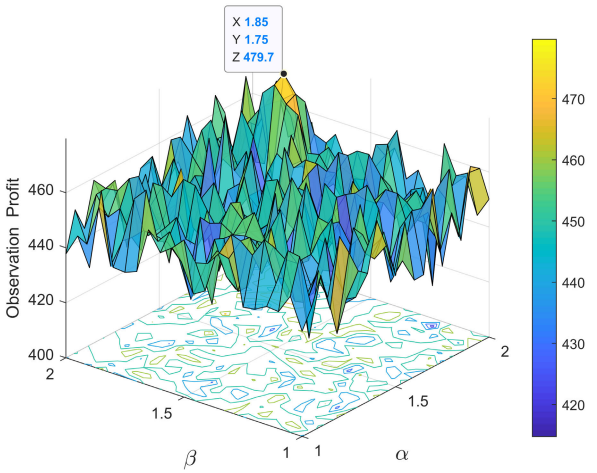

FIGURE 7. Early convergence result of profit under different heuristic factors.

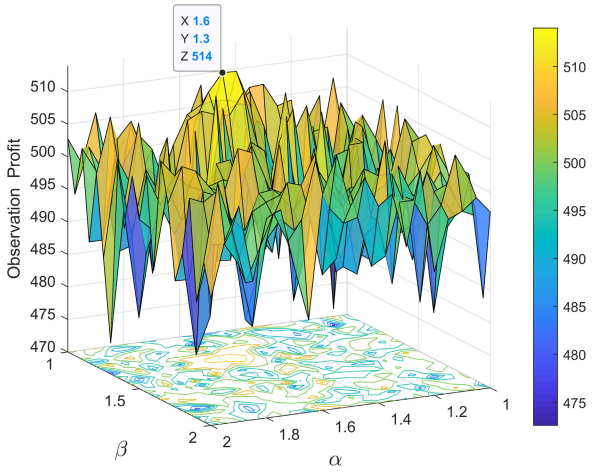

FIGURE 8. Late convergence result of profit under different heuristic factors.

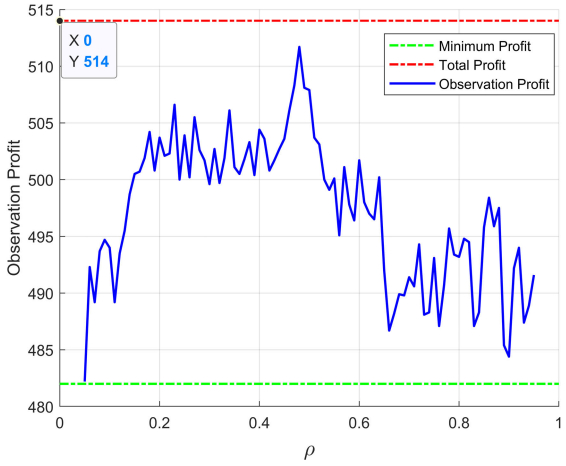

FIGURE 9. Late convergence result of profit under different heuristic factors.

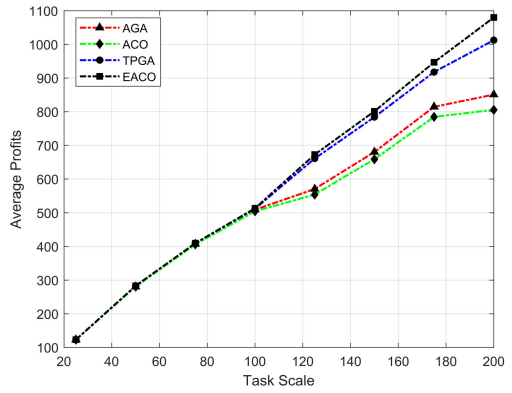

(a) Observation profits of different target scenarios

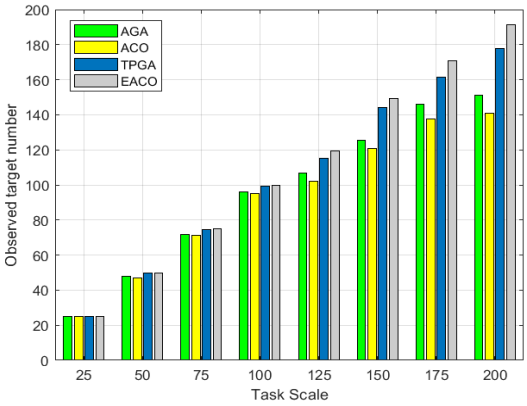

(b) Number of targets observed in different target scenarios

FIGURE 10. Results of multi-EOSs scheduling with different methods.

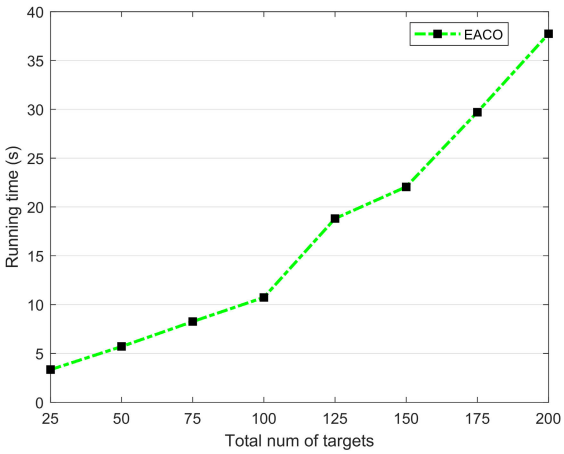

FIGURE 11. Number of missions performed by each EOS in the first stage.

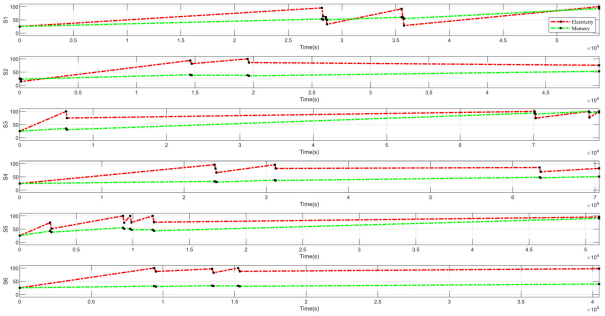

(a) Resource consumption and supplement of EOSs $S_1 - S_6$

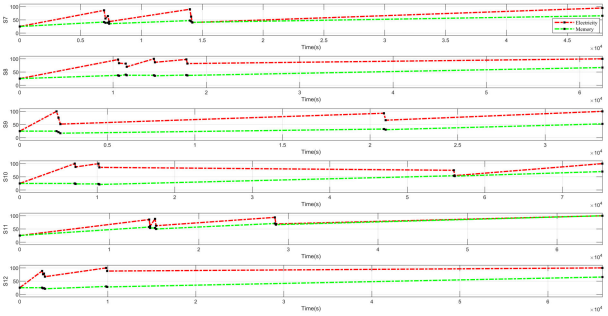

(b) Resource consumption and supplement of EOSs $S_7 - S_{12}$

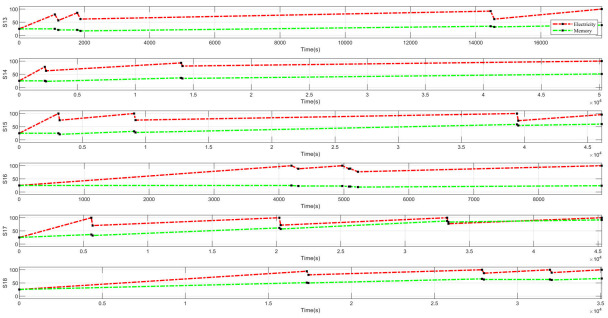

(c) Resource consumption and supplement of EOSs $S_{13} - S_{18}$

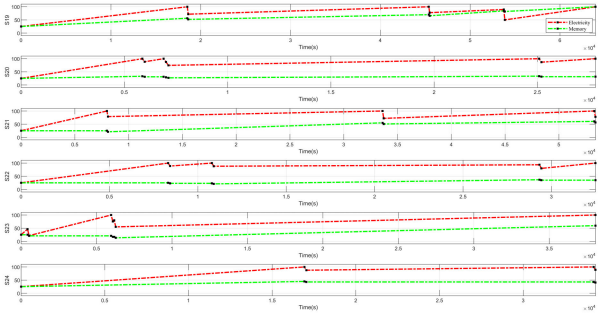

(d) Resource consumption and supplement of EOSs $S_{19} - S_{24}$

FIGURE 12. Results of multi-EOSs scheduling with different methods.

converge to a better solution. The yellow parts indicate that the average values of the objective functions were larger, implying that the algorithm produced better results. As can be seen in Fig. 7, when α and β, the average values of the first 10 iterations of the algorithm were the larger. Therefore, the heuristic factors in the early stage of EACO were set as α_0 and β_0, which is helpful for the algorithm to converge to a better solution. As shown in Fig. 8, when $\alpha \in [1.55, 1.65]$ and $\beta \in [1.25, 1.35]$, EACO has a better optimal solution. Therefore, the later adjustment strategy of EACO is set to $\alpha = 1.6$ and $\beta = 1.3$.

The value of the evaporation factor also affects the convergence of the algorithm, so we chose from $\rho \in [0.05, 0.95]$

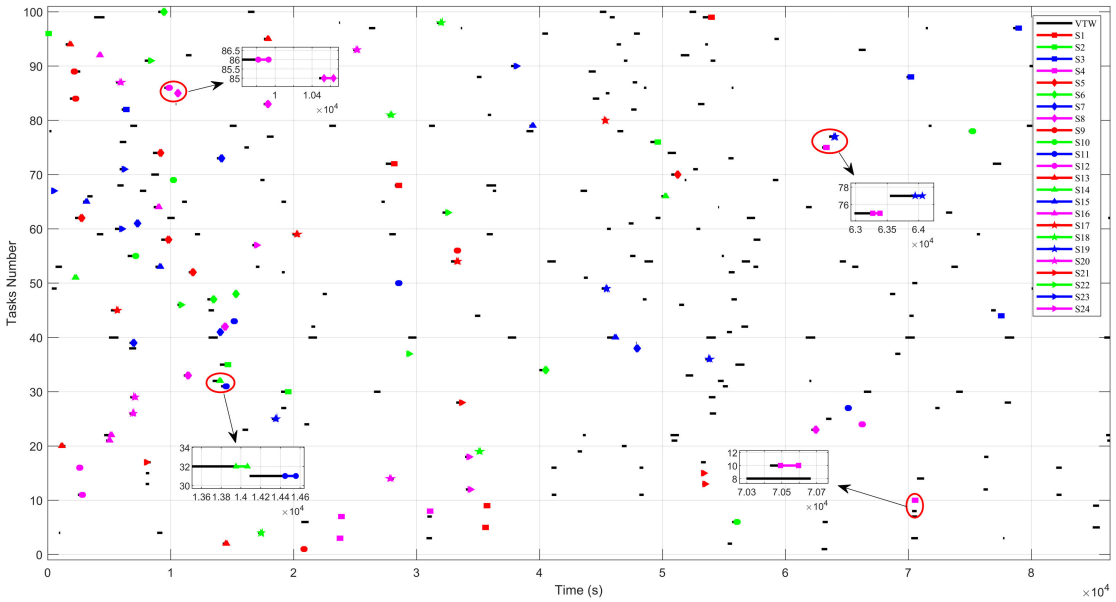

FIGURE 13. Results of mission pre-planning for each EOS.

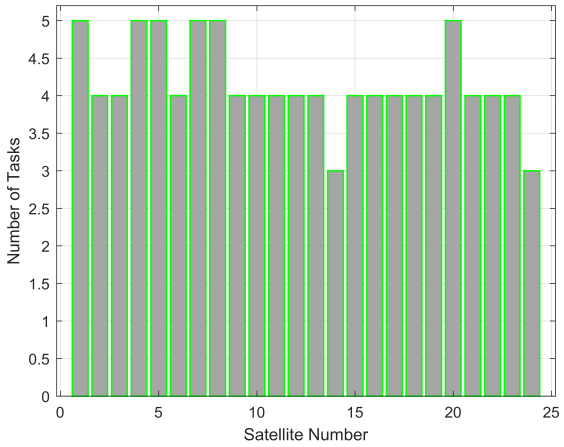

FIGURE 14. Number of missions performed by each EOS in the first stage.

with an interval of 0.01 and repeat the calculation 20 times under each parameter.

Different values of the evaporation factor have different influences on EACO. It can be seen from Fig. 9 that the evaporation factor has good convergence when this value is about 0.5.

B. COMPARISON WITH DIFFERENT ALGORITHMS

To further verify the effectiveness of the proposed algorithm, we compared the EACO with the two-phase genetic annealing algorithm (TPGA) [14], adaptive GA (AGA), and ACO for the above eight target scenarios. The AGA considers that the crossover probability and mutation probability will change with the fitness function. To fully describe the effects of the algorithms, each algorithm was repeated 20 times.

It can be seen from Fig. 10 that the four algorithms obtain better scheduling schemes when the number of targets is small. Only the sum of the priorities of the observed missions is larger, which indicates that the scheduling scheme is better, and the algorithm does not converge earlier. However, with the increase in the scale of the targets, the observed targets and the observation profits obtained by the adaptive GA and ACO are gradually reduced, which infers that the two algorithms may fall into local optimum. The TPGA and EACO can achieve better results, but the EACO produces better observation profits and observes more targets at a large scale compared with the TPGA.

TABLE 4. First stage: missions execution sequence of each EOS.

Satellite Number	Missions sequence
1	$T_{72} \rightarrow T_{68} \rightarrow T_5 \rightarrow T_9 \rightarrow T_{99}$
2	$T_{96} \rightarrow T_{35} \rightarrow T_{30} \rightarrow T_{76}$
3	$T_{82} \rightarrow T_{88} \rightarrow T_{44} \rightarrow T_{97}$
4	$T_3 \rightarrow T_7 \rightarrow T_8 \rightarrow T_{75} \rightarrow T_{10}$
5	$T_{62} \rightarrow T_{74} \rightarrow T_{58} \rightarrow T_{52} \rightarrow T_{70}$
6	$T_{100} \rightarrow T_{47} \rightarrow T_{48} \rightarrow T_{34}$
7	$T_{39} \rightarrow T_{61} \rightarrow T_{41} \rightarrow T_{73} \rightarrow T_{38}$
8	$T_{85} \rightarrow T_{33} \rightarrow T_{42} \rightarrow T_{83} \rightarrow T_{23}$
9	$T_{89} \rightarrow T_{84} \rightarrow T_1 \rightarrow T_{56}$
10	$T_{55} \rightarrow T_{69} \rightarrow T_6 \rightarrow T_{78}$
11	$T_{31} \rightarrow T_{43} \rightarrow T_{50} \rightarrow T_{27}$
12	$T_{16} \rightarrow T_{11} \rightarrow T_{86} \rightarrow T_{24}$
13	$T_{20} \rightarrow T_{94} \rightarrow T_2 \rightarrow T_{95}$
14	$T_{51} \rightarrow T_{32} \rightarrow T_{66}$
15	$T_{65} \rightarrow T_{53} \rightarrow T_{79} \rightarrow T_{40}$
16	$T_{92} \rightarrow T_{21} \rightarrow T_{22} \rightarrow T_{64}$
17	$T_{45} \rightarrow T_{59} \rightarrow T_{54} \rightarrow T_{80}$
18	$T_4 \rightarrow T_{81} \rightarrow T_{98} \rightarrow T_{19}$
19	$T_{25} \rightarrow T_{49} \rightarrow T_{36} \rightarrow T_{77}$
20	$T_{87} \rightarrow T_{26} \rightarrow T_{29} \rightarrow T_{93} \rightarrow T_{14}$
21	$T_{17} \rightarrow T_{28} \rightarrow T_{15} \rightarrow T_{13}$
22	$T_{91} \rightarrow T_{46} \rightarrow T_{37} \rightarrow T_{63}$
23	$T_{67} \rightarrow T_{60} \rightarrow T_{71} \rightarrow T_{90}$
24	$T_{57} \rightarrow T_{18} \rightarrow T_{12}$

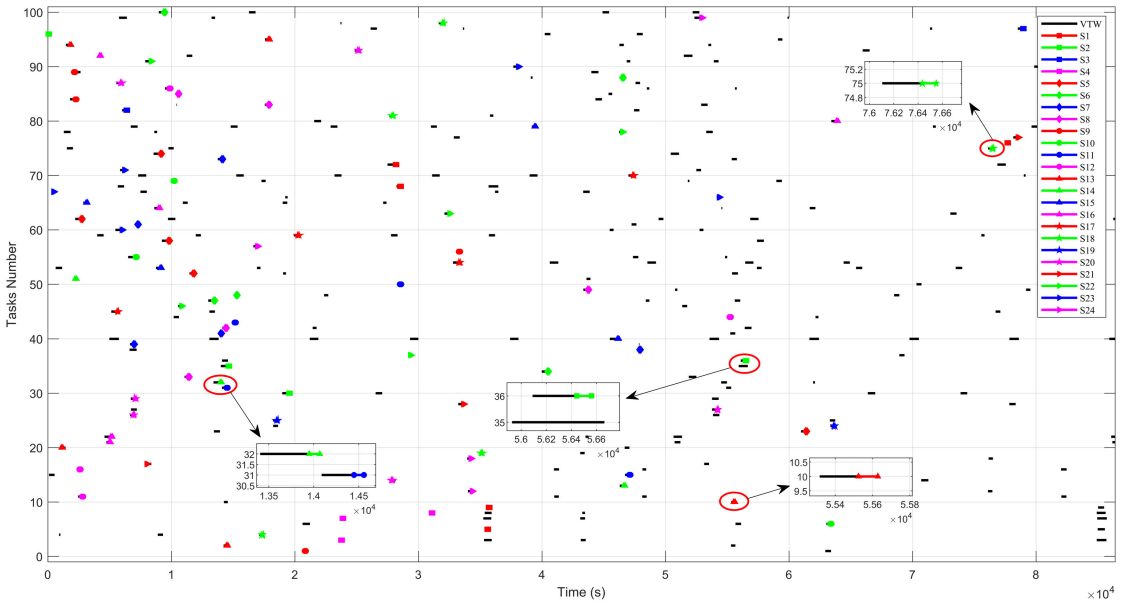

FIGURE 15. Results of mission replanning for each EOS.

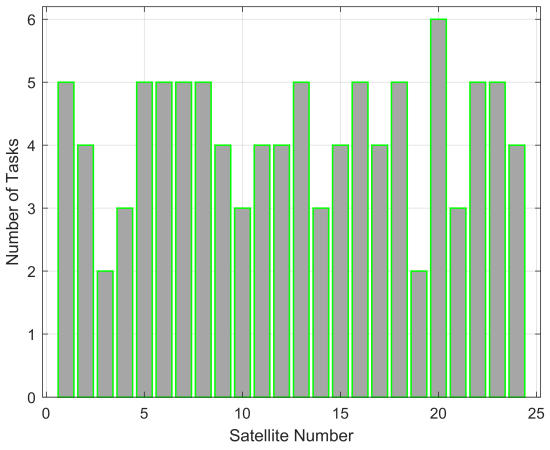

FIGURE 16. Number of missions performed by each EOS in the second stage.

The first stage is mission pre-planning, which can obtain the scheduling results of each EOS offline, because the key data can be obtained by STK in advance, which can save a lot of time. The running time of the EACO under different mission sizes is presented in Fig.11. To describe the scheduling state of each EOS, taking target scenario (d) as an example, the mission executions of 24 earth resource satellites for 100 ground targets are described. The scheduling results of the first stage for multiple EOSs in scenario (d) are presented in Fig. 12 Fig. 13 and Fig. 14, which show the process of image acquisition, consumption and supplement of electricity and memory.

Fig. 12 shows the remaining resources for each satellite during their mission. During multi-EOSs mission scheduling, both imaging and data transmission consume a certain amount of electricity and memory; however, considering the

TABLE 5. Second stage: missions execution sequence of each EOS.

Satellite Number	Missions sequence
1	$T_{72} \rightarrow T_{68} \rightarrow T_5 \rightarrow T_9 \rightarrow T_{76}$
2	$T_{96} \rightarrow T_{35} \rightarrow T_{30} \rightarrow T_{36}$
3	$T_{82} \rightarrow T_{97}$
4	$T_3 \rightarrow T_7 \rightarrow T_8$
5	$T_{62} \rightarrow T_{74} \rightarrow T_{58} \rightarrow T_{52} \rightarrow T_{23}$
6	$T_{100} \rightarrow T_{47} \rightarrow T_{48} \rightarrow T_{34} \rightarrow T_{88}$
7	$T_{39} \rightarrow T_{61} \rightarrow T_{41} \rightarrow T_{73} \rightarrow T_{38}$
8	$T_{85} \rightarrow T_{33} \rightarrow T_{42} \rightarrow T_{83} \rightarrow T_{49}$
9	$T_{89} \rightarrow T_{84} \rightarrow T_1 \rightarrow T_{56}$
10	$T_{55} \rightarrow T_{69} \rightarrow T_6$
11	$T_{31} \rightarrow T_{43} \rightarrow T_{50} \rightarrow T_{15}$
12	$T_{16} \rightarrow T_{11} \rightarrow T_{86} \rightarrow T_{44}$
13	$T_{20} \rightarrow T_{94} \rightarrow T_2 \rightarrow T_{95} \rightarrow T_{10}$
14	$T_{51} \rightarrow T_{32} \rightarrow T_{13}$
15	$T_{65} \rightarrow T_{53} \rightarrow T_{79} \rightarrow T_{40}$
16	$T_{92} \rightarrow T_{21} \rightarrow T_{22} \rightarrow T_{64} \rightarrow T_{80}$
17	$T_{45} \rightarrow T_{59} \rightarrow T_{54} \rightarrow T_{70}$
18	$T_4 \rightarrow T_{81} \rightarrow T_{98} \rightarrow T_{19} \rightarrow T_{75}$
19	$T_{25} \rightarrow T_{24}$
20	$T_{87} \rightarrow T_{26} \rightarrow T_{29} \rightarrow T_{93} \rightarrow T_{14} \rightarrow T_{27}$
21	$T_{17} \rightarrow T_{28} \rightarrow T_{77}$
22	$T_{91} \rightarrow T_{46} \rightarrow T_{37} \rightarrow T_{63} \rightarrow T_{78}$
23	$T_{67} \rightarrow T_{60} \rightarrow T_{71} \rightarrow T_{90} \rightarrow T_{66}$
24	$T_{57} \rightarrow T_{18} \rightarrow T_{12} \rightarrow T_{99}$

importance of solar energy and the ground stations, the EACO can enable each EOS to complete more missions with limited resources and balance the workload of each EOS.

Fig. 13 and Fig. 14 show the results of multi-EOSs mission scheduling in the first stage. The low orbit of the EOS allows it to orbit the earth many times in a day, so it can observe some missions on the ground many times. The ordinate is the mission number from 1 to 100 and the horizontal axis is the time of day. In Fig. 13, the black line is the VTWs of EOS for the allocated mission, and the red, green, blue and

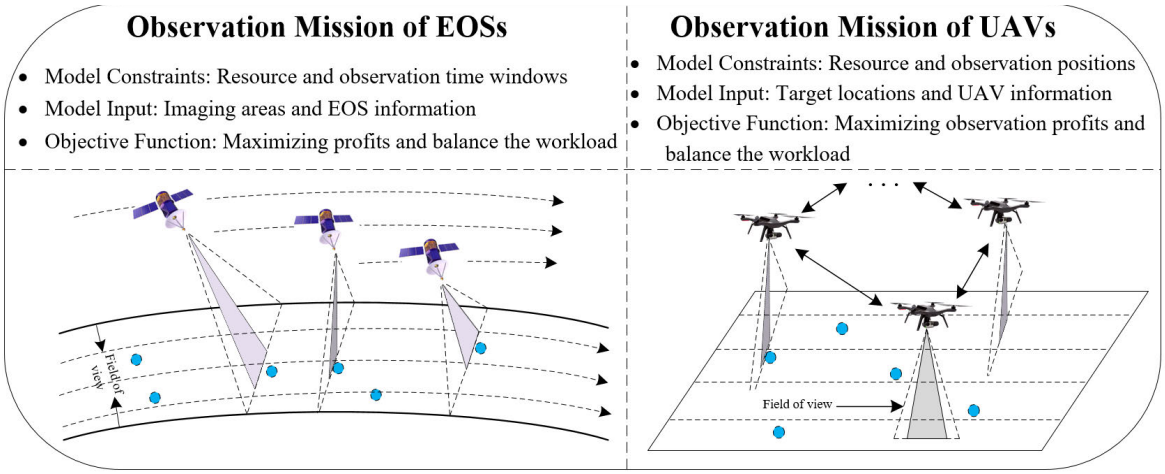

FIGURE 17. Relationship between EOSs observation mission and UAVs observation mission.

pink lines are the execution time interval of each EOS. The scheduling result for 100 missions is plotted in Fig. 14. As can be seen from Fig. 12 (a) and Fig. 13, mission T_{75} is allocated to EOS S_4, and the execution time is about 63200 s, so the electricity and memory of S_4 are reduced in this time period. From Fig. 12 (b) and Fig. 13, it can be seen that EOS S_{11} performs mission T_{31} at around 14400 s and from Fig. 12 (b), it can be seen that the electricity and memory of EOS S_{11} are also consumed by the execution of missions. According to the pre-planning result of each EOS in Fig. 13, we can obtain the mission execution sequence of each EOS in Table 4.

In this study, we consider that the EOS sensors may fail during multi-EOSs mission, thereby preventing them from completing the allocated missions. Therefore, we propose ICNP and mission insertion mechanism for mission replanning. Assuming that EOS S_4 fails after 12 hours of operation, it can be seen from Fig. 13 that missions T_{10} and missions T_{75} pre-allocated to EOS S_4 need to be reallocated. Based on the interactive replanning approach, the results of multi-EOSs mission replanning are shown in Fig. 15 and Fig. 16.

Fig. 15 and Fig. 16 show the scheduling results of multiple EOSs based on the interactive replanning approach due to failure of EOS S_4. From Fig. 15, we can find that the missions originally scheduled to be executed after 12 hours are reallocated, and mission T_{10} and mission T_{75} are successfully allocated to EOS S_{13} and S_{18}, respectively. It can be seen from the local enlarged drawing in Fig. 15 that mission T_{10} is reallocated to EOS S_{13} at about 55600 s, and mission T_{75} is reallocated to EOS S_{18} at about 76500 s. The rescheduling result of 100 missions is shown in Fig. 16, which shows the number of missions performed by each EOS. According to the replanning result of each EOS in Fig. 15, we can obtain the missions execution sequence of each EOS in Table 5.

C. UAVs FLIGHT EXPERIMENT

To show the results of the operation of the multiple satellites in orbit, we use 24 quadrotor UAVs to simulate the multi-satellite earth observation mission based on the existing multi-UAV platform. Because UAVs can carry the pan-head cameras and capture the images of the mission area in real time, similar to the imaging processes of the EOSs. First, as shown in Fig. 5, it is assumed that there is an earth in the middle of the orbit of multiple UAVs, then the mission locations to be observed are set on the surface of the earth, and multiple UAVs operate according to the orbit of each satellite. When the UAV reaches the top of the pre-allocated mission, it can capture the target by adjusting the camera angle. Firstly, the motion information of each EOS is obtained by STK, and then the trajectory information of multiple UAVs is obtained by scaling it in a certain proportion. The relationship between EOSs observation mission and UAVs observation mission are shown in Fig. 17.

FIGURE 18. Long-exposure photo of a flight with multi-UAVs.

To improve the viewing effect, we use the light of UAVs to show the trajectory of UAVs at night. In the simulation process, 24 EOSs are used to perform the observation missions. Here we use 24 UAVs to simulate the in-orbit observation process of EOSs. Fig. 18 depicts a long-exposure photo of a flight with multiple UAVs. The video of the experiment can be found at `https://www.youtube.com/watch?v=v0T_NFixHRY`.

TABLE 6. Specific parameters of multiple EOSs.

ID	Satellite	Two-Line Element Sets	$SE_l\,(J)$	$SM_l\,(MB)$
1	HAIYANG-2A	1 37781U 11043A 20360.00000000 .00000021 00000-0 20304-4 0 00005 2 37781 099.3166 004.2965 0000825 135.0189 070.7590 13.78724579471306	20000	16384
2	IRS-P6	1 28051U 03046A 20360.00000000 -.00000974 00000-0 -34180-3 0 00004 2 28051 098.4672 072.9166 0057913 180.2863 038.6458 14.34176297893691	10000	8192
3	SHIYAN 1	1 28220U 04012A 20360.00000000 .00000509 00000-0 40720-4 0 00006 2 28220 097.8664 330.9723 0018057 349.1572 035.9075 15.00177199909170	20000	16384
4	LAPAN-TUBSAT	1 29709U 07001A 20360.00000000 .00000094 00000-0 11838-4 0 00007 2 29709 097.8885 316.5839 0011850 207.1291 112.1709 14.82253009754580	10000	8192
5	HAIYANG 1B	1 31113U 07010A 20360.00000000 .00000017 00000-0 64643-5 0 00007 2 31113 098.3813 035.8031 0014243 013.9505 108.1154 14.30257729715395	20000	16384
6	YAOGAN 3	1 32289U 07055A 20360.00000000 .00000097 00000-0 12524-4 0 00009 2 32289 097.9836 014.1425 0001818 089.0377 120.3373 14.81054454709198	10000	8192
7	HUANJING 1A	1 33320U 08041A 20360.00000000 -.00000096 00000-0 -13514-4 0 00003 2 33320 097.7627 045.1114 0026481 168.1339 035.9355 14.77097957662739	20000	16384
8	HUANJING 1B	1 33321U 08041B 20360.00000000 .00000203 00000-0 28352-4 0 00008 2 33321 097.7709 047.6548 0034103 199.3281 149.5041 14.77304064662735	10000	8192
9	GOSAT (IBUKI)	1 33492U 09002A 20360.00000000 .00000150 00000-0 26487-4 0 00003 2 33492 098.0762 108.1293 0001230 092.9489 131.6818 14.67547667638093	20000	16384
10	RASAT	1 37791U 11044D 20360.00000000 .00000098 00000-0 18362-4 0 00002 2 37791 098.1096 090.1598 0022818 032.5726 187.8375 14.64802378500131	10000	8192
11	WORLDVIEW-3	1 40115U 14048A 20360.00000000 .00000629 00000-0 73618-4 0 00008 2 40115 097.8308 071.3951 0002327 075.3683 122.6194 14.85182463345087	20000	16384
12	YAOGAN 21	1 40143U 14053A 20360.00000000 .00001165 00000-0 48817-4 0 00004 2 40143 097.4184 064.8597 0015699 326.5777 111.7386 15.23480994000353	10000	8192
13	ASNARO	1 40298U 14070A 20360.00000000 .00001468 00000-0 69013-4 0 00001 2 40298 097.4070 078.7201 0001713 068.6722 085.7239 15.19668336340278	20000	16384
14	GAOFEN 9-01	1 40894U 15047A 20360.00000000 .00000137 00000-0 19678-4 0 00002 2 40894 097.8761 074.6998 0033467 150.9971 080.5316 14.76292192284597	10000	8192
15	LAPAN-A2	1 40931U 15052B 20360.00000000 .00000056 00000-0 78131-5 0 00000 2 40931 005.9986 056.6070 0013695 090.9618 168.1114 14.76656468283476	20000	16384
16	YAOGAN 29	1 41038U 15069A 20360.00000000 .00000057 00000-0 75076-5 0 00003 2 41038 098.0257 347.8212 0001855 041.5696 128.4747 14.80476935274470	10000	8192
17	KENT RIDGE 1	1 41167U 15077B 20360.00000000 .00000358 00000-0 21697-4 0 00008 2 41167 014.9767 177.3474 0011347 119.3642 251.2034 15.09248702277618	20000	16384
18	SCD 2	1 25504U 98060A 20360.00000000 .00000034 00000-0 96484-5 0 00006 2 25504 024.9939 149.9545 0017103 255.1722 116.2423 14.44110343170885	10000	8192
19	BIROS	1 41604U 16040F 20360.00000000 .00000812 00000-0 35324-4 0 00002 2 41604 097.2905 052.0137 0010639 232.1493 337.7834 15.22288688250350	20000	16384
20	GAOFEN 3	1 41727U 16049A 20360.00000000 .00000007 00000-0 20192-5 0 00001 2 41727 098.4113 004.9535 0001674 091.3338 348.1370 14.42215973230346	10000	8192
21	SKYSAT-C11	1 42987U 17068A 20360.00000000 .00003326 00000-0 86362-4 0 00009 2 42987 097.2461 111.7582 0011429 083.7046 083.5350 15.38947000175386	20000	16384
22	NUSAT-4 (ADA)	1 43195U 18015D 20360.00000000 .00002118 00000-0 84423-4 0 00008 2 43195 097.4638 127.7556 0017880 143.3072 012.0562 15.25115902160923	10000	8192
23	GAOFEN 10R	1 44622U 19066A 20360.00000000 .00000207 00000-0 27067-4 0 00009 2 44622 097.8388 298.7126 0001875 059.2886 221.6001 14.80600698066171	20000	16384
24	GAOFEN 12	1 44819U 19082A 20360.00000000 .00000074 00000-0 97364-5 0 00005 2 44819 097.9000 019.1721 0001943 078.8810 024.7132 14.80234660058144	10000	8192

VI. CONCLUSION

In this study, we investigated multi-EOSs autonomous scheduling by simultaneously considering observation, resource recoverability, and unexpected emergencies. A complete multi-EOSs scheduling scheme composed of two coupling stages, namely mission pre-planning and mission replanning, was proposed. To obtain the optimal observation scheme for multi-EOSs pre-planning, we developed cooperation and competition mechanisms as well as a dynamic adjustment approach to improve the quality of solutions.

To solve the urgent mission, an interactive replanning approach was proposed to reallocate the unfinished missions of the failed EOS. We conducted experiments in two stages of multi-EOSs scheduling to verify the effectiveness of the proposed algorithms. The first experiment compares our EACO with TSGA, AGA and ACO. The results show that EACO is superior over the other three in terms of both the number of observation missions and observation profits. Taking mission scenario (d) as an example, the mission execution time interval and resource change of each EOS are described in detail. In the second experiment, tasks that cannot be completed by the faulty EOS are reasonably allocated to other EOSs based on the interaction framework, and the observation profits are not reduced. Because the imaging process of UAV is similar to that of EOS, we used UAVs to simulate the operations of EOSs in orbit and obtained images of a region of interest using an airborne camera.

In our future work, we intend to include additional constraints, such as uncertainties due to clouds and weather effects, on the observations.

APPENDIX A

The specific parameters of each EOS are calculated by using SGP4 model and they are listed in Table 6. In addition, we set the following upper bound for the electricity and memory of each EOS.

REFERENCES

[1] G. S. Percivall, N. S. Alameh, H. Caumont, K. L. Moe, and J. D. Evans, "Improving disaster management using earth observations—GEOSS and CEOS activities," *IEEE J. Sel. Topics Appl. Earth Observ. Remote Sens.*, vol. 6, no. 3, pp. 1368–1375, Jun. 2013.

[2] A. Marx and G. O. Tetteh, "A forest vitality and change monitoring tool based on RapidEye imagery," *IEEE Geosci. Remote Sens. Lett.*, vol. 14, no. 6, pp. 801–805, Jun. 2017.

[3] A. Y. Hou, R. K. Kakar, S. Neeck, A. A. Azarbarzin, C. D. Kummerow, M. Kojima, R. Oki, K. Nakamura, and T. Iguchi, "The global precipitation measurement mission," *Bull. Amer. Meteorol. Soc.*, vol. 95, pp. 701–722, May 2014.

[4] E. Gill, P. Sundaramoorthy, J. Bouwmeester, B. Zandbergen, and R. Reinhard, "Formation flying within a constellation of nano-satellites: The QB50 mission," *Acta Astronautica*, vol. 82, no. 1, pp. 110–117, 2013.

[5] X. Zhang, M. Wu, W. Liu, X. Li, S. Yu, C. Lu, and J. Wickert, "Initial assessment of the COMPASS/BeiDou-3: New-generation navigation signals," *J. Geodesy*, vol. 91, no. 10, pp. 1225–1240, Oct. 2017.

[6] Y. Rizk, M. Awad, and E. W. Tunstel, "Cooperative heterogeneous multi-robot systems: A survey," *ACM Comput. Surv.*, vol. 52, no. 2, pp. 1–31, 2019.

[7] J. Wang, E. Demeulemeester, X. Hu, D. Qiu, and J. Liu, "Exact and heuristic scheduling algorithms for multiple earth observation satellites under uncertainties of clouds," *IEEE Syst. J.*, vol. 13, no. 3, pp. 3556–3567, Sep. 2019.

[8] X. Chen, G. Reinelt, G. Dai, and A. Spitz, "A mixed integer linear programming model for multi-satellite scheduling," *Eur. J. Oper. Res.*, vol. 275, no. 2, pp. 694–707, Jun. 2019.

[9] R. Pellerin, N. Perrier, and F. Berthaut, "A survey of hybrid metaheuristics for the resource-constrained project scheduling problem," *Eur. J. Oper. Res.*, vol. 280, no. 2, pp. 395–416, 2020.

[10] A. K. Kar, "Bio inspired computing—A review of algorithms and scope of applications," *Expert Syst. Appl.*, vol. 59, pp. 20–32, Oct. 2016.

[11] V. V. Darnopykh and V. V. Malyshev, "Operative planning of functional sessions for multisatellite observation and communication systems," *Acta Astronautica*, vol. 73, pp. 193–205, Apr. 2012.

[12] P. Tangpattanakul, N. Jozefowiez, and P. Lopez, "A multi-objective local search heuristic for scheduling earth observations taken by an agile satellite," *Eur. J. Oper. Res.*, vol. 245, no. 2, pp. 542–554, Sep. 2015.

[13] Z. Zheng, J. Guo, and E. Gill, "Distributed onboard mission planning for multi-satellite systems," *Aerosp. Sci. Technol.*, vol. 89, pp. 111–122, Jun. 2019.

[14] Z. Waiming, H. Xiaoxuan, X. Wei, and J. Peng, "A two-phase genetic annealing method for integrated earth observation satellite scheduling problems," *Soft Comput.*, vol. 23, no. 1, pp. 181–196, Jan. 2019.

[15] H. Kim and Y. K. Chang, "Mission scheduling optimization of SAR satellite constellation for minimizing system response time," *Aerosp. Sci. Technol.*, vol. 40, pp. 17–32, Jan. 2015.

[16] X. N. Nin, H. Tang, and L. X. Wu, "Satellite scheduling of large areal tasks for rapid response to natural disaster using a multi-objective genetic algorithm," *Int. J. Disaster Risk Reduction*, vol. 23, pp. 813–825, Jun. 2018.

[17] Y. Chen, M. Xu, X. Shen, G. Zhang, Z. Lu, and J. Xu, "A multi-objective modeling method of multi-satellite imaging task planning for large regional mapping," *Remote Sens.*, vol. 12, no. 3, p. 344, Jan. 2020.

[18] A. Sarkheyli, A. Bagheri, B. Ghorbani-Vaghei, and R. Askari-Moghadam, "Using an effective tabu search in interactive resources scheduling problem for LEO satellites missions," *Aerosp. Sci. Technol.*, vol. 29, no. 1, pp. 287–295, Aug. 2013.

[19] G. H. Wu, H. L. Wang, P. Witold, H. F. Li, and L. Wang, 'Satellite observation scheduling with a novel adaptive simulated annealing algorithm and a dynamic task clustering strategy," *Comput. Ind. Eng.*, vol. 113, pp. 576–588, Nov. 2017.

[20] Z. Zhang, F. Hu, and N. Zhang, "Ant colony algorithm for satellite control resource scheduling problem," *Int. J. Speech Technol.*, vol. 48, no. 10, pp. 3295–3305, Oct. 2018.

[21] Z. Zhang, N. Zhang, and Z. Feng, "Multi-satellite control resource scheduling based on ant colony optimization," *Expert Syst. Appl.*, vol. 41, no. 6, pp. 2816–2823, May 2014.

[22] Y. Yu, Q. Hou, J. Zhang, and W. Zhang, "Mission scheduling optimization of multi-optical satellites for multi-aerial targets staring surveillance," *J. Franklin Inst.*, vol. 357, no. 13, pp. 8657–8677, Sep. 2020.

[23] X.-Q. Chen and J. Yu, "Optimal mission planning of GEO on-orbit refueling in mixed strategy," *Acta Astronautica*, vol. 133, pp. 63–72, Apr. 2017.

[24] Y. Han, J. Luo, and X. Xu, "On the constellation design of multi-GNSS reflectometry mission using the particle swarm optimization algorithm," *Atmosphere*, vol. 10, no. 12, p. 807, Dec. 2019.

[25] J. Lu, Y. Chen, and R. He, "A learning-based approach for agile satellite onboard scheduling," *IEEE Access*, vol. 8, pp. 16941–16952, 2020.

[26] L. Ren, X. Ning, and J. Li, "Hierarchical reinforcement-learning for real-time scheduling of agile satellites," *IEEE Access*, vol. 8, pp. 220523–220532, 2020.

[27] Y. Du, T. Wang, B. Xin, L. Wang, Y. Chen, and L. Xing, "A data-driven parallel scheduling approach for multiple agile earth observation satellites," *IEEE Trans. Evol. Comput.*, vol. 24, no. 4, pp. 679–693, Aug. 2020.

[28] E. Stoll, A. Brunn, K. Shahid, and A. Horstmann, "The optimization of memory management in earth observation constellations," *Acta Astronautica*, vol. 164, pp. 433–443, Nov. 2019.

[29] J. Zhang, L. Xing, G. Peng, F. Yao, and C. Chen, "A large-scale multiobjective satellite data transmission scheduling algorithm based on SVM+NSGA-II," *Swarm Evol. Comput.*, vol. 50, Nov. 2019, Art. no. 100560.

[30] M. A. Mosa, A. S. Anwar, and A. Hamouda, "A survey of multiple types of text summarization with their satellite contents based on swarm intelligence optimization algorithms," *Knowl.-Based Syst.*, vol. 163, pp. 518–532, Jan. 2019.

[31] A. Prakasam and N. Savarimuthu, "Metaheuristic algorithms and probabilistic behaviour: A comprehensive analysis of ant colony optimization and its variants," *Artif. Intell. Rev.*, vol. 45, no. 1, pp. 97–130, Jan. 2016.

[32] J. Wang, X. Zhu, D. Qiu, and L. T. Yang, "Dynamic scheduling for emergency tasks on distributed imaging satellites with task merging," *IEEE Trans. Parallel Distrib. Syst.*, vol. 25, no. 9, pp. 2275–2285, Sep. 2014.

[33] L. J. He, J. D. Li, and M. Sheng, "Dynamic scheduling of hybrid tasks with time windows in data relay satellite networks," *IEEE Trans. Veh. Technol.*, vol. 25, no. 9, pp. 2275–2285, Mar. 2014.

JUNTONG QI received the B.S. degree from Tianjin University, China, in 2004, and the Ph.D. degree in control engineering from the Shenyang Institute of Automation, Chinese Academy of Sciences, in 2009. From 2011 to 2015, he was an Associate Research Fellow/Research Fellow with the Shenyang Institute of Automation, Chinese Academy of Sciences. He is currently a Professor with the School of Electrical and Information Engineering, Tianjin University, Tianjin, China. His research interests include intelligent optimization, cooperative control and multi-agent systems.

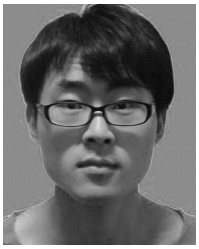

JINJIN GUO is currently pursuing the Ph.D. degree in control science and engineering from the School of Electrical and Information Engineering, Tianjin University, Tianjin, China. His research interests include intelligent optimization and multi-satellites task scheduling.

MINGMING WANG received the B.S. degree from Henan University in 2008, and the M.S. and Ph.D. degrees from the Shenyang Institute of Automation, Chinese Academy of Sciences, in 2010 and 2016, respectively. She is currently a Lecturer with the School of Electrical and Information Engineering, Tianjin University, Tianjin, China. Her current research interests include image processing and multi-agent systems.

CHONG WU received the B.S. degree from the Huazhong University of Science and Technology, in 2008, and the M.S. and Ph.D. degrees from the Shenyang Institute of Automation, Chinese Academy of Sciences, in 2010 and 2015, respectively. He is currently a Director of research and development with EFY Intelligent Control (Tianjin) Technology Company Ltd. His research interests include autonomous control and multi-agent systems.